

This is a copy of the published version, or version of record, available on the publisher's website. This version does not track changes, errata, or withdrawals on the publisher's site.

Nodeless superconductivity in noncentrosymmetric LaRhSn

Z. Y. Nie, J. W. Shu, A. Wang, H. Su, W. Y. Duan, A. D. Hillier, D. T. Adroja, P. K. Biswas, T. Takabatake, M. Smidman, and H. Q. Yuan

Published version information

Citation: ZY Nie et al. Nodeless superconductivity in noncentrosymmetric LaRhSn. Phys Rev B 105, no. 13 (2022): 134523.

DOI: [10.1103/PhysRevB.105.134523](https://doi.org/10.1103/PhysRevB.105.134523)

This version is made available in accordance with publisher policies. Please cite only the published version using the reference above. This is the citation assigned by the publisher at the time of issuing the APV. Please check the publisher's website for any updates.

This item was retrieved from **ePubs**, the Open Access archive of the Science and Technology Facilities Council, UK. Please contact epublications@stfc.ac.uk or go to <http://epubs.stfc.ac.uk/> for further information and policies.

Nodeless superconductivity in noncentrosymmetric LaRhSn

Z. Y. Nie,^{1,2} J. W. Shu,^{1,2} A. Wang,^{1,2} H. Su,^{1,2} W. Y. Duan,^{1,2} A. D. Hillier,³ D. T. Adroja,^{3,4} P. K. Biswas,³ T. Takabatake,^{5,6} M. Smidman,⁵ and H. Q. Yuan^{1,2,6,†}

¹Center for Correlated Matter and School of Physics, Zhejiang University, Hangzhou 310058, China

²Zhejiang Province Key Laboratory of Quantum Technology and Device, Department of Physics, Zhejiang University, Hangzhou 310058, China

³ISIS Facility, STFC Rutherford Appleton Laboratory, Harwell Science and Innovation Campus, Oxfordshire OX11 0QX, United Kingdom

⁴Highly Correlated Matter Research Group, Physics Department, University of Johannesburg, P.O. Box 524, Auckland Park 2006, South Africa

⁵Department of Quantum Matter, AdSE, Hiroshima University, Higashi-Hiroshima 739-8530, Japan

⁶State Key Laboratory of Silicon Materials, Zhejiang University, Hangzhou 310058, China



(Received 31 January 2022; revised 18 March 2022; accepted 18 April 2022; published 28 April 2022)

The superconducting order parameter of the noncentrosymmetric superconductor LaRhSn is investigated by means of low-temperature measurements of the specific heat, muon-spin relaxation/rotation (μ SR), and the tunnel-diode oscillator (TDO)-based method. The specific heat and magnetic penetration depth [$\lambda(T)$] show an exponentially activated temperature dependence, demonstrating fully gapped superconductivity in LaRhSn. The temperature dependences of $\lambda^{-2}(T)$ deduced from the TDO-based method and μ SR show nearly identical behavior, which can be well described by a single-gap s -wave model, with a zero-temperature gap value of $\Delta(0) = 1.77(4)k_B T_c$. The zero-field μ SR spectra do not show detectable changes upon cooling below T_c , and therefore there is no evidence for time-reversal-symmetry breaking in the superconducting state.

DOI: [10.1103/PhysRevB.105.134523](https://doi.org/10.1103/PhysRevB.105.134523)

I. INTRODUCTION

Noncentrosymmetric superconductors (NCSs) have attracted considerable interest, since in the absence of inversion symmetry, an antisymmetric potential gradient gives rise to an antisymmetric spin-orbit coupling (ASOC). The ASOC lifts the twofold spin degeneracy of the electronic bands, potentially allowing for unconventional superconducting properties such as the admixture of spin-singlet and spin-triplet pairing states [1,2]. In the noncentrosymmetric heavy fermion superconductor CePt₃Si, measurements of the magnetic penetration depth, thermal conductivity, and specific heat showed the presence of line nodes in the energy gap [3–5], and nodal superconductivity was subsequently found in other NCSs, such as Li₂Pt₃B [6,7], Y₂C₃ [8], K₂Cr₃As₃ [9,10], and ThCoC₂ [11]. However, many NCSs are found to be fully gapped superconductors, such as Mo₃Al₂C [12,13], RTSi₃ ($R = \text{La, Sr, Ba, Ca}$; $T = \text{transition metal}$) [14–18], BiPd [19,20], Re₆T [21–23], La₇T₃ [24,25], BeAu [26], and PbTaSe₂ [27–29]. Even though some of these systems have been found to have multiple superconducting gaps, many NCSs show evidence for single-gap s -wave superconductivity, indicating negligible contributions from a spin-triplet pairing component. The predominance of such s -wave superconductivity even in systems with strong ASOC has posed the question as to what conditions are required to give rise

to mixed parity pairing. In addition, even in NCSs exhibiting unconventional properties, unambiguously demonstrating the presence of singlet-triplet mixing remains challenging, and obtaining direct evidence may require probing associated topological superconducting phenomena such as gapless edge modes and Majorana modes [30,31].

Time-reversal-symmetry breaking (TRSB) has been observed in the superconducting states of some weakly correlated NCSs, such as LaNiC₂ [32], La₇T₃ [24,25], and several Re-based superconductors [21,33,34]. TRSB has primarily been revealed by muon-spin relaxation measurements, which detect the spontaneous appearance of small magnetic fields in the superconducting state, even in the absence of external applied fields [35]. In most cases, such systems have been found to have nodeless superconducting gaps, which has often been difficult to reconcile with the unconventional nature of the pairing state implied by TRSB. On the other hand, different behavior was recently found in the weakly correlated NCS CaPtAs, where there is evidence for both nodal superconductivity and TRSB [36,37]. Consequently, it is important to survey a wide range of different classes of NCSs, so as to look for novel behaviors arising from ASOC, as well as to reveal the origin of any time-reversal-symmetry breaking and to understand its relationship to the broken inversion symmetry.

LaRhSn crystallizes in the noncentrosymmetric hexagonal ZrNiAl-type structure (space group $P62m$) displayed in the inset of Fig. 1, where the rare-earth atoms form a distorted kagome lattice. Compounds in this family with a magnetic rare-earth atom have been extensively studied due

*Corresponding author: [msmidman@zju.edu.cn](mailto:mamidman@zju.edu.cn)

†Corresponding author: hqyuan@zju.edu.cn

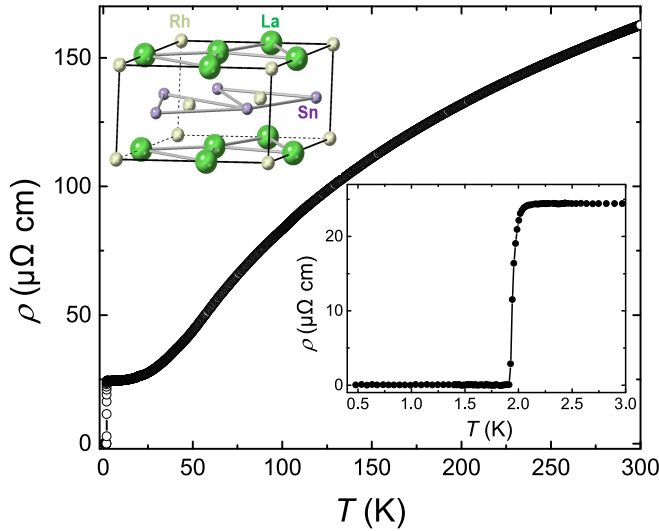


FIG. 1. Temperature dependence of the electrical resistivity $\rho(T)$ of LaRhSn from room temperature down to 0.5 K. The insets show $\rho(T)$ near the superconducting transition, and the crystal structure of LaRhSn.

to the interplay of strong electronic correlations and frustrated magnetism [38–40], while several other systems with nonmagnetic rare-earth elements are superconductors. For example, Sc(Ir,Rh)P, LaRhSn, and LaPdIn are superconductors with relatively low transition temperatures T_c [41–44], while (Zr,Hf)RuP, ZrRu(As,Si), and Mo(Ni,Ru)P have T_c 's over 10 K [45–49], where the higher T_c values may be a consequence of the phonon spectra and electron-phonon coupling strengths [47,50,51]. In this paper, we study the order parameter of LaRhSn via measurements of the electronic specific heat and magnetic penetration depth, where the latter is probed using both the tunnel-diode oscillator (TDO)-based method and muon-spin rotation (μ SR). The experimental results obtained by various techniques can be consistently described by a single-gap *s*-wave model corresponding to weak electron-phonon coupling. In addition, zero-field μ SR measurements do not exhibit detectable changes below T_c , and therefore there is no evidence for TRSB in the superconducting state.

II. EXPERIMENTAL DETAILS

Single crystals of LaRhSn were synthesized using the Czochralski method, as described in Ref. [52]. The specific heat was measured in a Quantum Design Physical Property Measurement System (PPMS) with a ^3He insert. The resistivity $\rho(T)$ was measured in a ^3He cryostat from room temperature down to 0.5 K, using a standard four-probe method. μ SR measurements were performed using the MuSR spectrometer at the ISIS pulsed muon source of the Rutherford Appleton Laboratory, U.K. [53,54]. The μ SR experiments were conducted in transverse-field (TF) and zero-field (ZF) configurations, so as to probe the flux-line lattice (FLL) and the presence or absence of time-reversal-symmetry breaking, respectively. Powdered single crystals of LaRhSn were mounted on a high-purity silver sample holder, which was mounted on a dilution refrigerator, with a temperature range

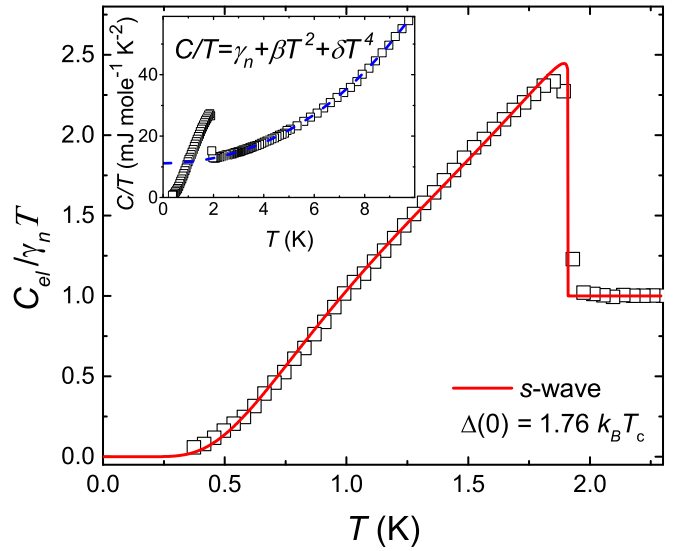


FIG. 2. Temperature dependence of the electronic specific heat as $C_{el}(T)/\gamma_n T$ of LaRhSn, where the solid line represents fitting with a single-gap *s*-wave model. The inset displays the total specific heat $C(T)/T$, where the dashed line represents the fitting to the normal state contribution.

from 0.05 to 2.5 K. With an active compensation system, the stray magnetic field at the sample position can be canceled to within 1 μT . TF- μ SR experiments were carried out in several fields up to 60 mT.

The shift of the magnetic penetration depth from the zero-temperature value $\Delta\lambda(T) = \lambda(T) - \lambda(0)$ was measured down to 0.3 K in a ^3He cryostat, using a tunnel-diode oscillator (TDO)-based method [55–57], with an operating frequency of 7 MHz and a noise level of 0.1 Hz. Samples with typical dimensions of $550 \times 450 \times 300 \mu\text{m}^3$ were mounted on a sapphire rod. The generated ac field is about 2 μT , which is much smaller than the lower critical field H_{c1} , ensuring that the sample remains in the Meissner state. $\Delta\lambda(T)$ is proportional to the frequency shift from zero-temperature $\Delta f(T)$, i.e., $\Delta\lambda(T) = G\Delta f(T)$, where G is the calibration factor determined from the geometry of the coil and sample [56].

III. RESULTS

A. Electrical resistivity and specific heat

The single crystals of LaRhSn were characterized by measurements of the electrical resistivity and specific heat. Figure 1 displays the electrical resistivity $\rho(T)$ from room temperature down to 0.5 K, which exhibits metallic behavior in the normal state. The inset shows $\rho(T)$ at low temperatures, where there is a sharp superconducting transition at around 2.0 K.

The inset of Fig. 2 displays the total specific heat $C(T)/T$ of LaRhSn in zero field, where there is a clear superconducting transition with a midpoint $T_c = 1.9$ K, in line with the behavior of $\rho(T)$. In the normal state, the specific heat data are fitted by $C(T)/T = \gamma_n + \beta T^2 + \delta T^4$, with $\gamma_n = 11.15(4) \text{ mJ mol}^{-1} \text{ K}^{-2}$, $\beta = 0.410(6) \text{ mJ mol}^{-1} \text{ K}^{-4}$, and $\delta = 0.87(1) \mu\text{J mol}^{-1} \text{ K}^{-6}$. Here, γ_n is the normal state Sommerfeld coefficient, and the latter two terms represent the

phonon contribution. The Debye temperature θ_D is estimated to be 241(1) K using $\theta_D = (12\pi^4 Rn/5\beta)^{1/3}$, where $R = 8.31 \text{ J mol}^{-1} \text{ K}^{-1}$ is the molar gas constant and $n = 3$ is the number of atoms per formula unit. The electron-phonon coupling constant $\lambda_{\text{el-ph}}$ can be approximated via

$$\lambda_{\text{el-ph}} = \frac{1.04 + \mu^* \ln\left(\frac{\theta_D}{1.45T_c}\right)}{(1 - 0.62\mu^*) \ln\left(\frac{\theta_D}{1.45T_c}\right) - 1.04}. \quad (1)$$

Using the typical values for μ^* of 0.1–0.15, $\lambda_{\text{el-ph}} = 0.47\text{--}0.57$ are obtained, close to the derived values for isostructural LaPdIn [44], indicating weakly coupled superconductivity in LaRhSn. In addition, the value of γ_n is very similar to that of LaPdIn, but larger than the values for LuPdIn and LaPtIn which are not superconducting down to at least 0.5 K [44]. This is consistent with the magnitude of the density of states at the Fermi level playing an important role in giving rise to superconductivity in this family of compounds.

The main panel of Fig. 2 shows the low-temperature electronic specific heat $C_{\text{el}}(T)/\gamma_n T$, from which the phonon contribution has been subtracted. In the superconducting state, the entropy S can be calculated by [60]

$$S = -\frac{3\gamma_n}{\pi^3} \int_0^{2\pi} \int_0^\infty [f \ln f + (1-f) \ln(1-f)] d\varepsilon d\phi, \quad (2)$$

where the $f(E, T) = [1 + \exp(E/k_B T)]^{-1}$ is the Fermi-Dirac distribution function. Here, $E = \sqrt{\varepsilon^2 + \Delta_k^2}$, where $\Delta_k(T) = \Delta(T)g_k$ is the superconducting gap function. Therefore, the electronic specific heat of the superconducting state can be obtained by $C_{\text{el}} = TdS/dT$. In the case of a single-gap s -wave model, there is no angle-dependent component ($g_k = 1$), and $\Delta(T)$ was approximated by [61]

$$\Delta(T) = \Delta(0) \tanh\{1.82[1.018(T_c/T - 1)]^{0.51}\}, \quad (3)$$

where $\Delta(0)$ is the zero-temperature superconducting gap magnitude. As shown by the solid line in Fig. 2, the zero-field $C_{\text{el}}/\gamma_n T$ can be well described by this single-gap s -wave model, with $\Delta(0) = 1.76(1)k_B T_c$.

Upon applying a magnetic field, the bulk superconducting transition is shifted to lower temperatures and is completely suppressed at about 0.25 T [see Fig. 3(a)]. The inset displays the extracted upper critical field $B_{c2}(T)$ and the corresponding fitting using the Werthamer-Helfand-Hohenberg (WHH) model [62], with a zero-temperature upper critical field $B_{c2}(0) = 0.219(2)$ T. Using $\lambda(0) = \sqrt{\Phi_0 B_{c2}(0)}/\sqrt{24\gamma_n \Delta(0)}$ [63], where the units of $B_{c2}(0)$ and γ_n are Gauss and ergs $\text{cm}^{-3} \text{ K}^{-2}$, respectively, a penetration depth at zero temperature $\lambda(0) = 244(1)$ nm is estimated using $\Delta(0) = 1.76(1)k_B T_c$. Combined with a Ginzburg-Landau (GL) coherence length of $\xi_{\text{GL}} = \sqrt{\Phi/2\pi B_{c2}(0)} = 38.7(2)$ nm, the GL parameter κ is estimated to be 6.30(4), indicating that LaRhSn is a type-II superconductor. Using the values of $\lambda(0) = 244(1)$ nm, a residual normal state resistivity $\rho_0 = 25 \mu\Omega \text{ cm}$, and $\gamma_n = 11.15(4) \text{ mJ mol}^{-1} \text{ K}^{-2}$, the mean free path ℓ and BCS coherence length ξ_{BCS} are estimated to be $\ell = 17.91(8)$ nm and $\xi_{\text{BCS}} = 43.8(2)$ nm [64]. The mean free path ℓ is smaller than ξ_{BCS} , indicating that the sample is in the dirty limit.

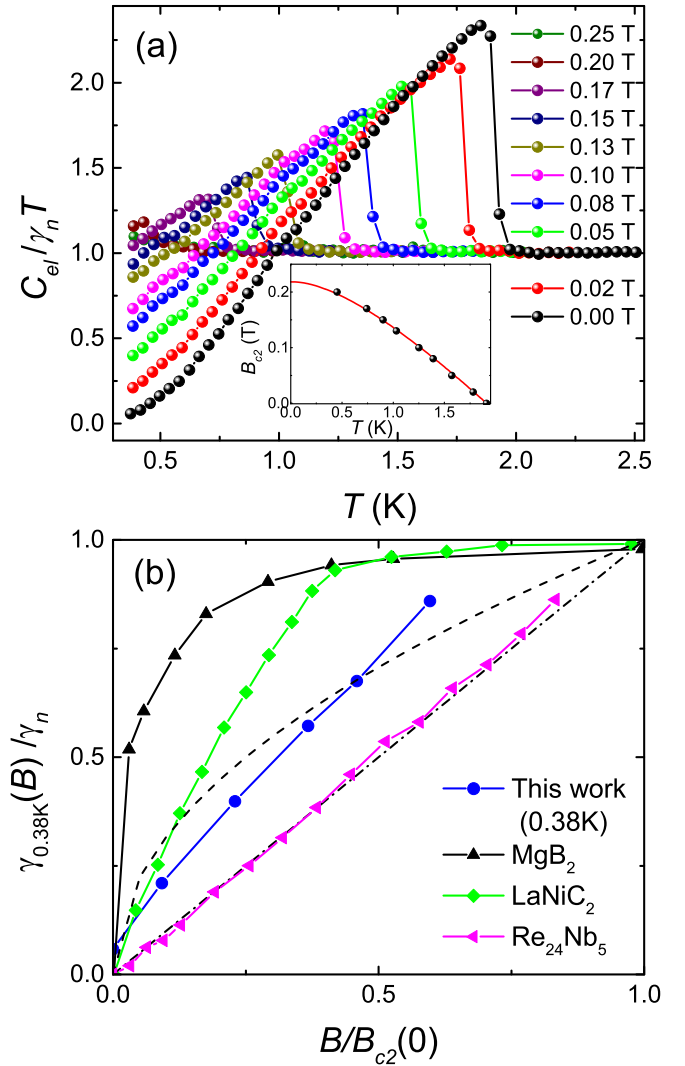


FIG. 3. (a) Temperature dependence of the electronic specific heat as $C_{\text{el}}/\gamma_n T$ of LaRhSn under various applied fields. The inset displays the temperature dependence of the upper critical field $B_{c2}(T)$, derived from the specific heat measurements, where the solid line represents fitting with the WHH model where $B_{c2}(0) = 0.219(2)$ T. (b) Field dependence of the residual Sommerfeld coefficient plotted as $\gamma_{0.38 \text{ K}}(B)/\gamma_n$ vs $B/B_{c2}(0)$ for LaRhSn, $\text{Re}_{24}\text{Nb}_5$ [34], MgB_2 [58], and LaNiC_2 [59]. The dashed and dashed-dotted lines correspond to the expected behaviors of nodal and single-gap s -wave superconductivity, respectively.

Figure 3(b) displays the field dependence of the Sommerfeld coefficient value at 0.38 K, normalized by its value in the normal state, i.e., $\gamma_{0.38 \text{ K}}(B)/\gamma_n$. It can be seen that $\gamma_{0.38 \text{ K}}(B)/\gamma_n$ shows a nearly linear field dependence, being similar to the fully gapped superconductor $\text{Re}_{24}\text{Nb}_5$ [34]. On the other hand, $\gamma_{0.38 \text{ K}}(B)/\gamma_n$ clearly deviates from the square-root field dependence (dashed line) expected for line nodal superconductors, as well as the typical behaviors of the multiband superconductors MgB_2 [58] and LaNiC_2 [59]. Note that $\gamma_{0.38 \text{ K}}(B)/\gamma_n$ of LaRhSn are determined from the specific heat at the lowest measured temperature, and therefore even in zero field the data have a finite value.

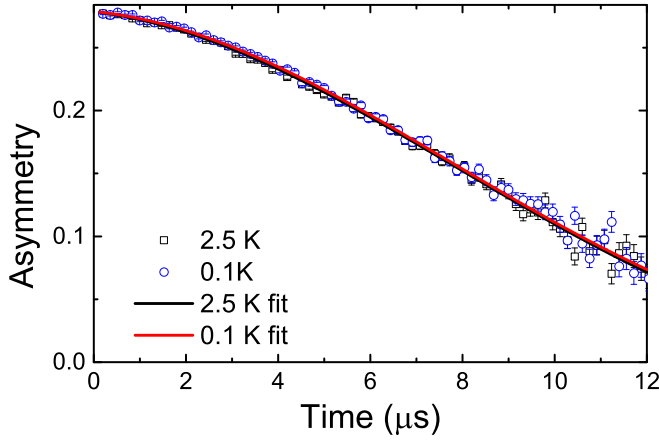


FIG. 4. ZF- μ SR spectra of LaRhSn at 2.5 K ($T > T_c$) and 0.1 K ($T < T_c$). The solid lines show the results from fitting using Eq. (4).

B. μ SR measurements

Figure 4 displays the zero-field (ZF) μ SR spectra collected at 2.5 K ($T > T_c$) and 0.1 K ($T < T_c$). These are fitted with a damped Gaussian Kubo-Toyabe (KT) function

$$G_{ZF}(t) = A \left[\frac{1}{3} + \frac{2}{3} (1 - \delta^2 t^2) \exp\left(-\frac{\delta^2 t^2}{2}\right) \right] \exp(-\Lambda t) + A_{bg}, \quad (4)$$

where A is the initial asymmetry, and A_{bg} corresponds to the time-independent background term from muons stopping in the silver sample holder. δ and Λ are the Gaussian and Lorentzian relaxation rates, respectively. Upon fitting with Eq. (4), $\delta = 0.086(3) \mu s^{-1}$ and $\Lambda = 0.0134(11) \mu s^{-1}$ were obtained at 2.5 K, while $\delta = 0.082(3) \mu s^{-1}$ and $\Lambda = 0.0157(10) \mu s^{-1}$ at 0.1 K. Therefore, we find no evidence for TRSB in the superconducting state of LaRhSn, and these results suggest that any spontaneous internal fields should be no larger than $6.6 \mu T$, which is smaller than the corresponding fields in other reported TRSB superconductors [35].

Transverse-field μ SR (TF- μ SR) measurements were carried out in the mixed state with applied fields in the range 40–60 mT, where the data were collected upon field cooling in order to probe a well-ordered flux-line lattice (FLL). The results at 2.5 and 0.05 K in a field of 40 mT are displayed in Fig. 5. The significant increase of the depolarization rate corresponds to the inhomogeneous field distribution in the sample, characteristic of the formation of a FLL. The TF- μ SR asymmetry were fitted to the sum of oscillations damped by Gaussian decaying functions

$$G_{TF}(t) = \sum_{i=1}^n A_i \cos(\gamma_\mu B_i t + \phi) e^{-(\sigma_i t)^2/2} + A_{BG}, \quad (5)$$

where A_i is the amplitude of the oscillating component, which precesses about a local field B_i with a common phase offset ϕ and a Gaussian decay rate σ_i , while $\gamma_\mu/2\pi = 135.5$ MHz/T and A_{BG} are the muon gyromagnetic ratio and background term, respectively. The asymmetry can be well fitted with three oscillatory components ($n = 3$), where σ_3 was fixed to zero, corresponding to muons stopping in the silver sample holder. Figure 6(a) displays the temperature dependence of $\sigma(T)$ obtained following the multiple-Gaussian method de-

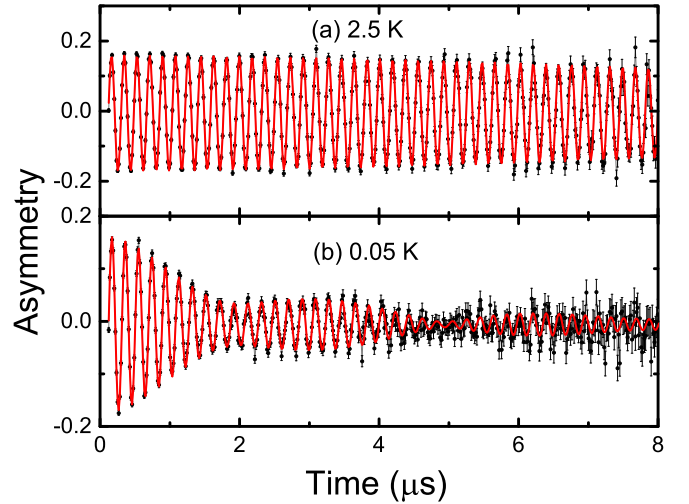


FIG. 5. Transverse-field μ SR spectra of LaRhSn at (a) 2.5 K ($T > T_c$) and (b) 0.05 K ($T < T_c$) in an applied field of 40 mT. The solid lines show the results of fitting with Eq. (5).

scribed in Ref. [65]. Here, the first and second moments of the field distribution are calculated as

$$\langle B \rangle = \sum_{i=1}^{n-1} \frac{A_i B_i}{A_1 + \dots + A_{n-1}}, \quad (6)$$

$$\langle B^2 \rangle = \sum_{i=1}^{n-1} \frac{A_i}{A_1 + \dots + A_{n-1}} [(\sigma_i/\gamma_\mu)^2 + [B_i - \langle B \rangle]^2], \quad (7)$$

and $\sigma = \gamma_\mu \sqrt{\langle B^2 \rangle}$. The relaxation rate in the normal state is ascribed to a temperature-independent contribution arising from quasistatic nuclear moments, with a nuclear dipolar relaxation rate $\sigma_N = 0.0851(27) \mu s^{-1}$. The superconducting component of the variance σ_{sc} is calculated as $\sigma_{sc} = \sqrt{\sigma^2 - \sigma_N^2}$, and its field dependence is displayed in Fig. 6(b) for several temperatures.

For small applied fields and large κ , σ_{sc} is field independent and proportional to λ^{-2} , which is not applicable for the current measurements of LaRhSn. On the other hand, for $\kappa \geq 5$ and $0.25/\kappa^{1.3} \leq b \leq 1$, σ_{sc} may be approximated by [66]

$$\sigma_{sc} = 4.854 \times 10^4 \frac{1}{\lambda^2} (1 - b) [1 + 1.21(1 - \sqrt{b})^3], \quad (8)$$

where $b = B/B_{c2}$ is the applied field normalized by the upper critical field. Since the κ of LaRhSn was determined to be about 6.30(4), the measurements of LaRhSn are within the applicability of Eq. (8). Therefore by fixing $B_{c2}(T)$ to the bulk values derived from the specific heat in Fig. 3, the temperature dependence of $\lambda^{-2}(T)$ can be obtained from fitting with Eq. (8) [Fig. 6(b)], and the results are shown in Fig. 8, together with the TDO results described in following section.

C. TDO measurements and superfluid density analysis

Figure 7 shows the penetration depth shift $\Delta\lambda(T)$ of LaRhSn at low temperatures, with a calibration factor $G = 14.2$ Å/Hz. The inset displays the frequency shift $\Delta f(T)$ from 2.5 K down to the base temperature of 0.3 K, where a sharp superconducting transition is observed at $T_c = 2$ K, in

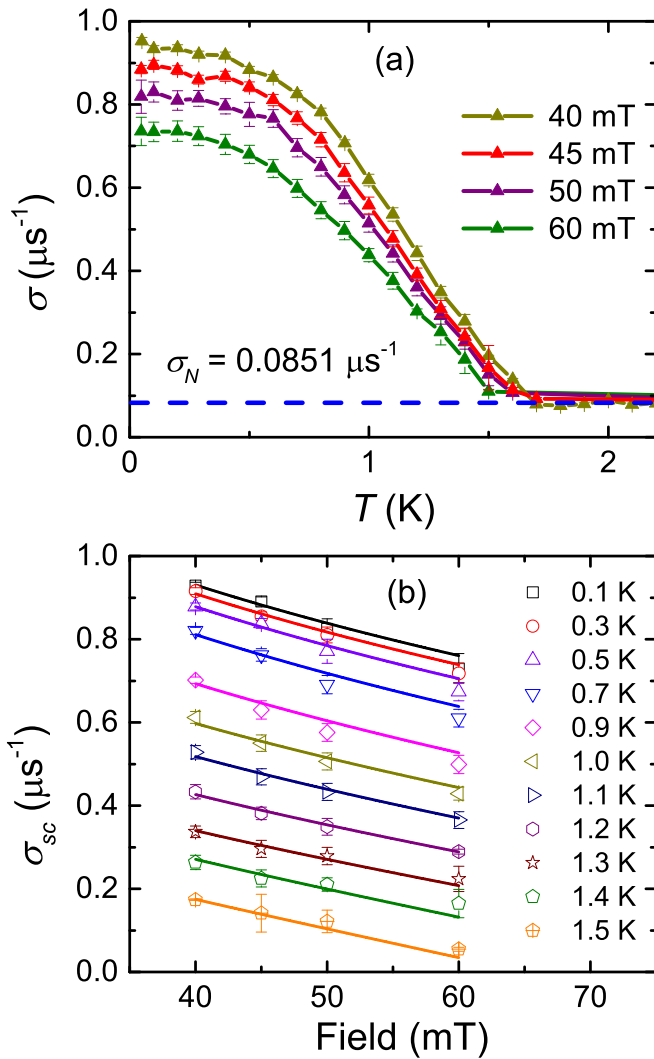


FIG. 6. (a) Temperature dependence of the Gaussian relaxation rate of the TF- μ SR spectra in different applied fields between 40 and 60 mT. (b) Field dependence of the superconducting contribution to the TF- μ SR relaxation rate σ_{sc} at various temperatures, where the solid lines correspond to fitting using Eq. (8).

accordance with other measurements. Upon further cooling, $\Delta\lambda(T)$ flattens at the lowest measured temperatures, indicating fully gapped superconductivity in LaRhSn. For an s -wave superconductor, the temperature dependence of $\Delta\lambda(T)$ for $T \ll T_c$ can be approximated by

$$\Delta\lambda(T) = \lambda(0) \sqrt{\frac{\pi \Delta(0)}{2k_B T}} \exp\left(-\frac{\Delta(0)}{k_B T}\right). \quad (9)$$

As shown by the solid line, the experimental data below $T_c/3$ can be well described by the s -wave model with $\Delta(0) = 1.80(1)k_B T_c$, where $\lambda(0) = 227.9$ nm was fixed to the value derived from TF- μ SR. The data were also fitted by a power-law dependence $\Delta\lambda(T) \propto T^n$, from 0.3 K up to 0.75 K. A large exponent of $n = 4.4$ is obtained, which is much larger than two, excluding nodal superconductivity in LaRhSn.

To further characterize the superconducting pairing state of LaRhSn, the temperature dependence of $\lambda^{-2}(T)$ was ana-

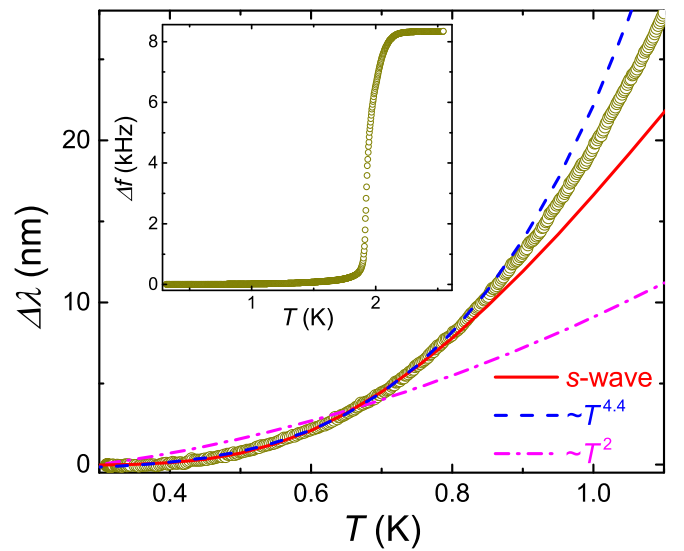


FIG. 7. The change of magnetic penetration depth $\Delta\lambda(T)$ of LaRhSn at low temperatures. The solid red, dashed blue, and dashed-dotted magenta lines represent fitting to an s -wave model, and power-law dependences $\sim T^{4.4}$ and $\sim T^2$, respectively. The inset displays the frequency shift $\Delta f(T)$ from 2.5 K down to 0.3 K, where there is a sharp superconducting transition at around $T_c = 2$ K.

lyzed, which is proportional to the superfluid density $\rho_s(T)$ as $\rho_s(T) = [\lambda(0)/\lambda(T)]^2$. Figure 8 displays $\lambda^{-2}(T)$ as a function of the reduced temperature T/T_c , where the data are derived from both the TDO and TF- μ SR measurements, which show nearly identical behavior. Since the previous analysis suggested that the sample is in the dirty limit, the results from TF- μ SR were fitted with the following expression for a dirty

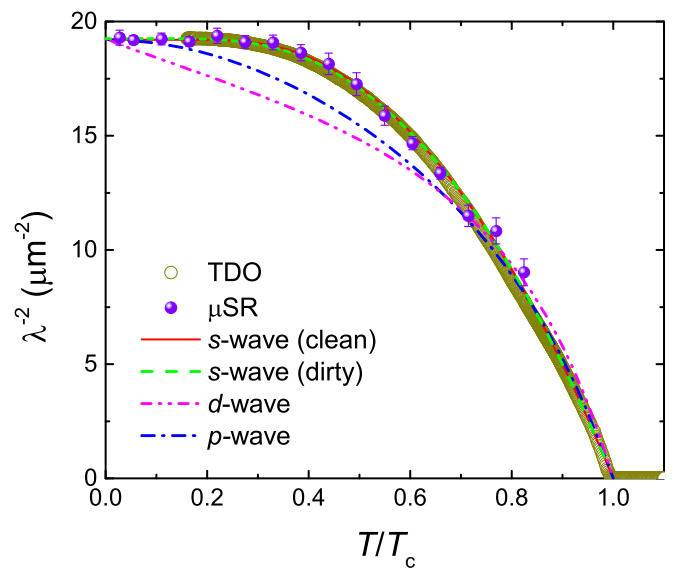


FIG. 8. Temperature dependence of $\lambda^{-2}(T)$ as a function of the normalized temperature T/T_c . The data are derived from measurements using the TDO-based method and TF- μ SR measurements, which correspond to the open circle and solid symbols, respectively. The lines show the results from fitting with different models for the gap structure.

TABLE I. Superconducting parameters of LaRhSn, where the parentheses with C and μ SR denote the results from the specific heat and μ SR, respectively.

Property	Unit	Value
T_c	K	1.9
$B_{c2}(0)$	T	0.219(2)
γ_n	mJ mol ⁻¹ K ⁻²	11.15(4)
Θ_D	K	241(1)
$\lambda_{\text{el-ph}}$		0.47–0.57
ξ_{GL}	nm	38.7(2)
ℓ	nm	17.91(8)
ξ_{BCS}	nm	43.8(2)
$\lambda_0(C)$	nm	244(1)
$\lambda_0(\mu\text{SR})^{\text{dirty}}$	nm	227.9(9)
$\kappa(C)$		6.30(4)
$\kappa(\mu\text{SR})^{\text{dirty}}$		5.89(4)
$\Delta(0)(C)$	$k_B T_c$	1.76(1)
$\Delta(0)(\mu\text{SR})^{\text{dirty}}$	$k_B T_c$	1.77(4)

s -wave model [67]

$$\rho_s(T) = \frac{\Delta(T)}{\Delta(0)} \tanh \left\{ \frac{\Delta(T)}{2k_B T} \right\}. \quad (10)$$

As shown by the dashed line in Fig. 8, the dirty s -wave model can well describe the experimental data, with $\lambda(0) = 227.9(9)$ nm and $\Delta(0) = 1.77(4)k_B T_c$. The data were also analyzed using the clean limit expression

$$\rho_s(T) = \frac{\lambda^{-2}(T)}{\lambda^{-2}(0)} = 1 + 2 \left\langle \int_{\Delta_k}^{\infty} \frac{E dE}{\sqrt{E^2 - \Delta_k^2}} \frac{\partial f}{\partial E} \right\rangle_{\text{FS}}, \quad (11)$$

where a clean single-gap s -wave model can also fit the data well, yielding a larger gap value of $\Delta(0) = 2.05(3)k_B T_c$. Here, the gap value obtained from the dirty s -wave model is in very good agreement to those derived from the analysis of specific heat and low-temperature $\Delta\lambda(T)$, while the clean limit value is considerably larger, which is in line with the previous dirty limit calculation. We note that due to the samples being in the dirty limit, we cannot exclude an anisotropic superconducting gap in LaRhSn, since impurity scattering can suppress any gap anisotropy. On the other hand, as also shown in Fig. 8, a d -wave model with $g_k = \cos 2\phi$ and p -wave model

with $g_k = \sin \theta$ ($\phi =$ azimuthal angle, $\theta =$ polar angle) cannot account for the data, further indicating a lack of nodal superconductivity in LaRhSn. Meanwhile, the value of $\lambda(0)$ obtained from μ SR experiments is very close to that from specific heat results. Using this value of $\lambda(0) = 227.9(9)$ nm, $\kappa = 5.89(4)$ is estimated, which corresponds well to the value from the specific heat analysis. The obtained superconducting parameters of LaRhSn are displayed in Table I. Therefore, the results of specific heat, TDO-based measurements, and μ SR can all be consistently described by a single-gap s -wave model with a gap magnitude very close to that of weak-coupling BCS theory, and there is no evidence for time-reversal-symmetry breaking below T_c .

IV. SUMMARY

In summary, we have studied the order parameter of the noncentrosymmetric superconductor LaRhSn. Both the specific heat and magnetic penetration depth show exponentially activated behavior at low temperatures, providing strong evidence for fully gapped superconductivity. $\lambda^{-2}(T)$ derived from the TDO-based method and TF- μ SR, as well as the specific heat can be consistently well described by a single-gap s -wave model, with a gap magnitude very close to that of weak coupling BCS theory. Together with findings for LaPdIn [44] and ZrRuAs [47], our results suggest that fully gapped s -wave superconductivity, together with a lack of evidence for time-reversal-symmetry breaking, are consistent common features of weakly correlated NCS with the ZrNiAl-type structure and there is a lack of significant singlet-triplet mixing.

ACKNOWLEDGMENTS

This work was supported by the National Key R&D Program of China (Grant No. 2017YFA0303100), the Key R&D Program of Zhejiang Province, China (Grant No. 2021C01002), the National Natural Science Foundation of China (Grants No. 11874320, No. 11974306, and No. 12034017), and the Zhejiang Provincial Natural Science Foundation of China (R22A0410240). D.T.A. would like to thank the Royal Society of London for Advanced Newton Fellowship funding between U.K. and China. Experiments at the ISIS Pulsed Neutron and Muon Source were supported by a beamtime allocation from the Science and Technology Facilities Council (Grant No. RB2010190 [54]).

- [1] L. P. Gor'kov and E. I. Rashba, Superconducting 2D System with Lifted Spin Degeneracy: Mixed Singlet-Triplet State, *Phys. Rev. Lett.* **87**, 037004 (2001).
- [2] M. Smidman, M. B. Salamon, H. Q. Yuan, and D. F. Agterberg, Superconductivity and spin-orbit coupling in noncentrosymmetric materials: a review, *Rep. Prog. Phys.* **80**, 036501 (2017).
- [3] I. Bonalde, W. Brämer-Escamilla, and E. Bauer, Evidence for Line Nodes in the Superconducting Energy Gap of Noncentrosymmetric CePt₃Si from Magnetic Penetration Depth Measurements, *Phys. Rev. Lett.* **94**, 207002 (2005).
- [4] K. Izawa, Y. Kasahara, Y. Matsuda, K. Behnia, T. Yasuda, R. Settai, and Y. Onuki, Line Nodes in the Superconducting Gap

Function of Noncentrosymmetric CePt₃Si, *Phys. Rev. Lett.* **94**, 197002 (2005).

- [5] T. Takeuchi, T. Yasuda, M. Tsujino, H. Shishido, R. Settai, H. Harima, and Y. Ōnuki, Specific heat and de Haas-van Alphen experiments on the heavy-fermion superconductor CePt₃Si, *J. Phys. Soc. Jpn.* **76**, 014702 (2007).
- [6] H. Q. Yuan, D. F. Agterberg, N. Hayashi, P. Badica, D. Vandervelde, K. Togano, M. Sigrüst, and M. B. Salamon, s -Wave Spin-Triplet Order in Superconductors without Inversion Symmetry: Li₂Pd₃B and Li₂Pt₃B, *Phys. Rev. Lett.* **97**, 017006 (2006).
- [7] M. Nishiyama, Y. Inada, and G. Q. Zheng, Spin Triplet Superconducting State due to Broken Inversion Symmetry in Li₂Pt₃B, *Phys. Rev. Lett.* **98**, 047002 (2007).

- [8] J. Chen, M. B. Salamon, S. Akutagawa, J. Akimitsu, J. Singleton, J. L. Zhang, L. Jiao, and H. Q. Yuan, Evidence of nodal gap structure in the noncentrosymmetric superconductor Y_2C_3 , *Phys. Rev. B* **83**, 144529 (2011).
- [9] J. K. Bao, J. Y. Liu, C. W. Ma, Z. H. Meng, Z. T. Tang, Y. L. Sun, H. F. Zhai, H. Jiang, H. Bai, C. M. Feng, Z. A. Xu, and G. H. Cao, Superconductivity in Quasi-One-Dimensional $K_2Cr_3As_3$ with Significant Electron Correlations, *Phys. Rev. X* **5**, 011013 (2015).
- [10] G. M. Pang, M. Smidman, W. B. Jiang, J. K. Bao, Z. F. Weng, Y. F. Wang, L. Jiao, J. L. Zhang, G. H. Cao, and H. Q. Yuan, Evidence for nodal superconductivity in quasi-one-dimensional $K_2Cr_3As_3$, *Phys. Rev. B* **91**, 220502(R) (2015).
- [11] A. Bhattacharyya, D. T. Adroja, K. Panda, S. Saha, T. Das, A. J. S. Machado, O. V. Cigarroa, T. W. Grant, Z. Fisk, A. D. Hillier, and P. Manfrinetti, Evidence of a Nodal Line in the Superconducting Gap Symmetry of Noncentrosymmetric $ThCoC_2$, *Phys. Rev. Lett.* **122**, 147001 (2019).
- [12] I. Bonalde, H. Kim, R. Prozorov, C. Rojas, P. Rogl, and E. Bauer, Evidence for conventional superconducting behavior in noncentrosymmetric Mo_3Al_2C , *Phys. Rev. B* **84**, 134506 (2011).
- [13] E. Bauer, C. Sekine, U. Sai, P. Rogl, P. K. Biswas, and A. Amato, Absence of time-reversal symmetry breaking in the noncentrosymmetric superconductor Mo_3Al_2C , *Phys. Rev. B* **90**, 054522 (2014).
- [14] E. Bauer, R. T. Khan, H. Michor, E. Royanian, A. Grytsiv, N. Melnychenko-Koblyuk, P. Rogl, D. Reith, R. Podlucky, E.-W. Scheidt, W. Wolf, and M. Marsman, $BaPtSi_3$: A noncentrosymmetric BCS-like superconductor, *Phys. Rev. B* **80**, 064504 (2009).
- [15] V. K. Anand, A. D. Hillier, D. T. Adroja, A. M. Strydom, H. Michor, K. A. McEwen, and B. D. Rainford, Specific heat and μ SR study on the noncentrosymmetric superconductor $LaRhSi_3$, *Phys. Rev. B* **83**, 064522 (2011).
- [16] M. Smidman, A. D. Hillier, D. T. Adroja, M. R. Lees, V. K. Anand, R. P. Singh, R. I. Smith, D. M. Paul, and G. Balakrishnan, Investigations of the superconducting states of noncentrosymmetric $LaPdSi_3$ and $LaPtSi_3$, *Phys. Rev. B* **89**, 094509 (2014).
- [17] F. Kneidinger, L. Salamakha, E. Bauer, I. Zeiringer, P. Rogl, C. Blaas-Schneider, D. Reith, and R. Podlucky, Superconductivity in noncentrosymmetric $BaAl_4$ derived structures, *Phys. Rev. B* **90**, 024504 (2014).
- [18] G. Eguchi, D. C. Peets, M. Kriener, Y. Maeno, E. Nishibori, Y. Kumazawa, K. Banno, S. Maki, and H. Sawa, Crystallographic and superconducting properties of the fully gapped noncentrosymmetric $5d$ -electron superconductors $CaMSi_3$ ($M = Ir, Pt$), *Phys. Rev. B* **83**, 024512 (2011).
- [19] L. Jiao, J. L. Zhang, Y. Chen, Z. F. Weng, Y. M. Shao, J. Y. Feng, X. Lu, B. Joshi, A. Thamizhavel, S. Ramakrishnan, and H. Q. Yuan, Anisotropic superconductivity in noncentrosymmetric $BiPd$, *Phys. Rev. B* **89**, 060507(R) (2014).
- [20] Z. Sun, M. Enayat, A. Maldonado, C. Lithgow, E. Yelland, D. C. Peets, A. Yaresko, A. P. Schnyder, and P. Wahl, Dirac surface states and nature of superconductivity in noncentrosymmetric $BiPd$, *Nat. Commun.* **6**, 6633 (2015).
- [21] R. P. Singh, A. D. Hillier, B. Mazidian, J. Quintanilla, J. F. Annett, D. M. Paul, G. Balakrishnan, and M. R. Lees, Detection of Time-Reversal Symmetry Breaking in the Noncentrosymmetric Superconductor Re_6Zr Using Muon-Spin Spectroscopy, *Phys. Rev. Lett.* **112**, 107002 (2014).
- [22] G. M. Pang, Z. Y. Nie, A. Wang, D. Singh, W. Xie, W. B. Jiang, Y. Chen, R. P. Singh, M. Smidman, and H. Q. Yuan, Fully gapped superconductivity in single crystals of noncentrosymmetric Re_6Zr with broken time-reversal symmetry, *Phys. Rev. B* **97**, 224506 (2018).
- [23] D. Singh, A. D. Hillier, A. Thamizhavel, and R. P. Singh, Superconducting properties of the noncentrosymmetric superconductor Re_6Hf , *Phys. Rev. B* **94**, 054515 (2016).
- [24] J. A. T. Barker, D. Singh, A. Thamizhavel, A. D. Hillier, M. R. Lees, G. Balakrishnan, D. M. Paul, and R. P. Singh, Unconventional Superconductivity in La_7Ir_3 Revealed by Muon Spin Relaxation: Introducing a New Family of Noncentrosymmetric Superconductor That Breaks Time-Reversal Symmetry, *Phys. Rev. Lett.* **115**, 267001 (2015).
- [25] D. Singh, M. S. Scheurer, A. D. Hillier, D. T. Adroja, and R. P. Singh, Time-reversal-symmetry breaking and unconventional pairing in the noncentrosymmetric superconductor La_7Rh_3 , *Phys. Rev. B* **102**, 134511 (2020).
- [26] A. Amon, E. Svanidze, R. Cardoso-Gil, M. N. Wilson, H. Rosner, M. Bobnar, W. Schnelle, J. W. Lynn, R. Gumenuik, C. Hennig, G. M. Luke, H. Borrmann, A. Leithe-Jasper, and Y. Grin, Noncentrosymmetric superconductor $BeAu$, *Phys. Rev. B* **97**, 014501 (2018).
- [27] C.-L. Zhang, Z. Yuan, G. Bian, S.-Y. Xu, X. Zhang, M. Z. Hasan, and S. Jia, Superconducting properties in single crystals of the topological nodal semimetal $PbTaSe_2$, *Phys. Rev. B* **93**, 054520 (2016).
- [28] G. M. Pang, M. Smidman, L. X. Zhao, Y. F. Wang, Z. F. Weng, L. Q. Che, Y. Chen, X. Lu, G. F. Chen, and H. Q. Yuan, Nodeless superconductivity in noncentrosymmetric $PbTaSe_2$ single crystals, *Phys. Rev. B* **93**, 060506(R) (2016).
- [29] M. N. Wilson, A. M. Hallas, Y. Cai, S. Guo, Z. Gong, R. Sankar, F. C. Chou, Y. J. Uemura, and G. M. Luke, μ SR study of the noncentrosymmetric superconductor $PbTaSe_2$, *Phys. Rev. B* **95**, 224506 (2017).
- [30] M. Sato and S. Fujimoto, Topological phases of noncentrosymmetric superconductors: Edge states, Majorana fermions, and non-Abelian statistics, *Phys. Rev. B* **79**, 094504 (2009).
- [31] M. Sato, Y. Takahashi, and S. Fujimoto, Non-Abelian topological orders and Majorana fermions in spin-singlet superconductors, *Phys. Rev. B* **82**, 134521 (2010).
- [32] A. D. Hillier, J. Quintanilla, and R. Cywinski, Evidence for Time-Reversal Symmetry Breaking in the Noncentrosymmetric Superconductor $LaNiC_2$, *Phys. Rev. Lett.* **102**, 117007 (2009).
- [33] T. Shang, G. M. Pang, C. Baines, W. B. Jiang, W. Xie, A. Wang, M. Medarde, E. Pomjakushina, M. Shi, J. Mesot, H. Q. Yuan, and T. Shiroka, Nodeless superconductivity and time-reversal symmetry breaking in the noncentrosymmetric superconductor $Re_{24}Ti_5$, *Phys. Rev. B* **97**, 020502(R) (2018).
- [34] T. Shang, M. Smidman, S. K. Ghosh, C. Baines, L. J. Chang, D. J. Gawryluk, J. A. T. Barker, R. P. Singh, D. M. Paul, G. Balakrishnan, E. Pomjakushina, M. Shi, M. Medarde, A. D. Hillier, H. Q. Yuan, J. Quintanilla, J. Mesot, and T. Shiroka, Time-Reversal Symmetry Breaking in Re-Based Superconductors, *Phys. Rev. Lett.* **121**, 257002 (2018).
- [35] S. K. Ghosh, M. Smidman, T. Shang, J. F. Annett, A. D. Hillier, J. Quintanilla, and H. Yuan, Recent progress on

- superconductors with time-reversal symmetry breaking, *J. Phys.: Condens. Matter* **33**, 033001 (2021).
- [36] W. Xie, P. R. Zhang, B. Shen, W. B. Jiang, G. M. Pang, T. Shang, C. Cao, M. Smidman, and H. Q. Yuan, CaPtAs: A new noncentrosymmetric superconductor, *Sci. China: Phys., Mech. Astron.* **63**, 237412 (2020).
- [37] T. Shang, M. Smidman, A. Wang, L.-J. Chang, C. Baines, M. K. Lee, Z. Y. Nie, G. M. Pang, W. Xie, W. B. Jiang, M. Shi, M. Medarde, T. Shiroka, and H. Q. Yuan, Simultaneous Nodal Superconductivity and Time-Reversal Symmetry Breaking in the Noncentrosymmetric Superconductor CaPtAs, *Phys. Rev. Lett.* **124**, 207001 (2020).
- [38] H. Zhao, J. Zhang, M. Lyu, S. Bachus, Y. Tokiwa, P. Gegenwart, S. Zhang, J. Cheng, Y.-f. Yang, G. Chen *et al.*, Quantum-critical phase from frustrated magnetism in a strongly correlated metal, *Nat. Phys.* **15**, 1261 (2019).
- [39] Y. Tokiwa, C. Stingl, M.-S. Kim, T. Takabatake, and P. Gegenwart, Characteristic signatures of quantum criticality driven by geometrical frustration, *Sci. Adv.* **1**, e1500001 (2015).
- [40] Y. Shimura, A. Wörl, M. Sundermann, S. Tsuda, D. T. Adroja, A. Bhattacharyya, A. M. Strydom, A. D. Hillier, F. L. Pratt, A. Gloskovskii, A. Severing, T. Onimaru, P. Gegenwart, and T. Takabatake, Antiferromagnetic Correlations in Strongly Valence Fluctuating CeIrSn, *Phys. Rev. Lett.* **126**, 217202 (2021).
- [41] F. Canepa and S. Cirafici, Equiatomic ternary lanthanum-transition metal-tin phases: structural and electrical results, *J. Alloys Compd.* **232**, 71 (1996).
- [42] Y. Okamoto, T. Inohara, Y. Yamakawa, A. Yamakage, and K. Takenaka, Superconductivity in the hexagonal ternary phosphide ScIrP, *J. Phys. Soc. Jpn.* **85**, 013704 (2016).
- [43] T. Inohara, Y. Okamoto, Y. Yamakawa, and K. Takenaka, Synthesis and superconducting properties of a hexagonal phosphide ScRhP, *J. Phys. Soc. Jpn.* **85**, 094706 (2016).
- [44] H. Su, Z. Y. Nie, F. Du, S. S. Luo, A. Wang, Y. J. Zhang, Y. Chen, P. K. Biswas, D. T. Adroja, C. Cao, M. Smidman, and H. Q. Yuan, Fully gapped superconductivity with preserved time-reversal symmetry in noncentrosymmetric LaPdIn, *Phys. Rev. B* **104**, 024505 (2021).
- [45] H. Barz, H. C. Ku, G. P. Meisner, Z. Fisk, and B. T. Matthias, Ternary transition metal phosphides: High-temperature superconductors, *Proc. Natl. Acad. Sci. USA* **77**, 3132 (1980).
- [46] G. Meisner, H. Ku, and H. Barz, Superconducting equiatomic ternary transition metal arsenides, *Mater. Res. Bull.* **18**, 983 (1983).
- [47] D. Das, D. T. Adroja, M. R. Lees, R. W. Taylor, Z. S. Bishnoi, V. K. Anand, A. Bhattacharyya, Z. Guguchia, C. Baines, H. Luetkens, G. B. G. Stenning, L. Duan, X. Wang, and C. Jin, Probing the superconducting gap structure in the noncentrosymmetric topological superconductor ZrRuAs, *Phys. Rev. B* **103**, 144516 (2021).
- [48] I. Shirotni, K. Tachi, Y. Konno, S. Todo, and T. Yagi, Superconductivity of the ternary ruthenium compounds HfRuP and ZrRuX (X = P, As, Si or Ge) prepared at a high pressure, *Philos. Mag. B* **79**, 767 (1999).
- [49] I. Shirotni, M. Tajaya, I. Kaneko, C. Sekine, and T. Yagi, Superconductivity of MRuP and MNiP (M = Mo or W) prepared at high pressure, *Solid State Commun.* **116**, 683 (2000).
- [50] A. Bhattacharyya, K. Panda, D. T. Adroja, N. Kase, P. K. Biswas, S. Saha, T. Das, M. R. Lees, and A. D. Hillier, Investigation of superconducting gap structure in HfIrSi using muon spin relaxation/rotation, *J. Phys.: Condens. Matter* **32**, 085601 (2020).
- [51] S. Bağcı, M. Cin, H. Y. Uzunok, E. Karaca, H. M. Tütüncü, and G. P. Srivastava, Investigating the normal state and superconducting state properties of orthorhombic and hexagonal ZrRuP: A first-principles study, *Phys. Rev. B* **100**, 184507 (2019).
- [52] H. Higaki, I. Ishii, D. Hirata, M. S. Kim, T. Takabatake, and T. Suzuki, Elastic, thermal, magnetic and transport properties of Kondo compounds CeRhIn and CeRhSn, *J. Phys. Soc. Jpn.* **75**, 024709 (2006).
- [53] *Muon Science: Muons in Physics, Chemistry and Materials*, edited by S. L. Lee, S. H. Kilcoyne, and R. Cywinski (SUSSP Publications and IOP Publishing, Bristol, UK, 1999).
- [54] M. Smidman, D. T. Adroja, Z. Y. Nie, A. D. Hillier, and P. Biswas, *Superconductivity of a Hexagonal Noncentrosymmetric Superconductor* (STFC ISIS Neutron and Muon Source, 2020), <https://doi.org/10.5286/ISIS.E.RB2010190-1>.
- [55] C. T. Van Degrift, Tunnel diode oscillator for 0.001 ppm measurements at low temperatures, *Rev. Sci. Instrum.* **46**, 599 (1975).
- [56] R. Prozorov, R. W. Giannetta, A. Carrington, and F. M. Araujo-Moreira, Meissner-London state in superconductors of rectangular cross section in a perpendicular magnetic field, *Phys. Rev. B* **62**, 115 (2000).
- [57] E. M. E. Chia, Penetration depth studies of unconventional superconductors, Ph.D. thesis, University of Illinois at Urbana Champaign, 2004.
- [58] F. Bouquet, R. A. Fisher, N. E. Phillips, D. G. Hinks, and J. D. Jorgensen, Specific Heat of Mg¹¹B₂: Evidence for a Second Energy Gap, *Phys. Rev. Lett.* **87**, 047001 (2001).
- [59] J. Chen, L. Jiao, J. L. Zhang, Y. Chen, L. Yang, M. Nicklas, F. Steglich, and H. Q. Yuan, Evidence for two-gap superconductivity in the non-centrosymmetric compound LaNiC₂, *New J. Phys.* **15**, 053005 (2013).
- [60] F. Bouquet, Y. Wang, R. A. Fisher, D. G. Hinks, J. D. Jorgensen, A. Junod, and N. E. Phillips, Phenomenological two-gap model for the specific heat of MgB₂, *Europhys. Lett.* **56**, 856 (2001).
- [61] A. Carrington and F. Manzano, Magnetic penetration depth of MgB₂, *Physica C* **385**, 205 (2003).
- [62] N. R. Werthamer, E. Helfand, and P. C. Hohenberg, Temperature and Purity Dependence of the Superconducting Critical Field, H_{c2} . III. Electron Spin and Spin-Orbit Effects, *Phys. Rev.* **147**, 295 (1966).
- [63] F. Gross, B. S. Chandrasekhar, D. Einzel, K. Andres, P. J. Hirschfeld, H. R. Ott, J. Beuers, Z. Fisk, and J. L. Smoth, Anomalous temperature dependence of the magnetic field penetration depth in superconducting UBe₁₃, *Z. Phys. B* **64**, 175 (1986).
- [64] T. P. Orlando, E. J. McNiff, S. Foner, and M. R. Beasley, Critical fields, Pauli paramagnetic limiting, and material parameters of Nb₃Sn and V₃Si, *Phys. Rev. B* **19**, 4545 (1979).
- [65] A. Maisuradze, R. Khasanov, A. Shengelaya, and H. Keller, Comparison of different methods for analyzing μ SR line shapes in the vortex state of type-II superconductors, *J. Phys.: Condens. Matter* **21**, 075701 (2009).
- [66] E. H. Brandt, Properties of the ideal Ginzburg-Landau vortex lattice, *Phys. Rev. B* **68**, 054506 (2003).
- [67] M. Tinkham, *Introduction to Superconductivity* (Courier Corporation, North Chelmsford, MA, 2004).